Journal of Physics and Its Applications

Journal homepage : https://ejournal2.undip.ac.id/index.php/jpa/index

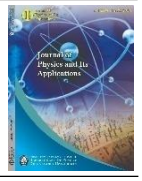

Performance Comparison of Large-Core Optical Waveguides with Waste-Derived and Analytical-Grade Chitosan Core Materials

Ian Yulianti[1], Aflah Agus Rizkika[1], Ngurah Made Darma Putra[1], Mohammad Alauhdin[2], Budi Astuti[1], Wasi Sakti Wiwit Prayitno[1], Deffrian Prayogo[1], Nishfa Mufatihah[1], and Naufal Athoriq[1]

[1]*Department of Physics, Faculty of Mathematics and Natural Sciences, Universitas Negeri Semarang, Semarang, Indonesia*
[2]*Department of Chemistry, Faculty of Mathematics and Natural Sciences, Universitas Negeri Semarang, Semarang, Indonesia*

**Corresponding author : ianyulianti@mail.unnes.ac.id*

ARTICLE INFO

Article history:
Received: 15 December 2025
Accepted: 27 January 2026
Available online: 27 February 2026

Keywords:
Optical waveguide
Biopolymer
Chitosan
PMMA cladding
Optical loss

ABSTRACT

This study investigates and compares the optical performance of large-core polymer waveguides fabricated using shrimp-shell-derived chitosan (SSC) and analytical-grade chitosan (AGC) as core materials. Both materials were processed into a buried square-core waveguide configuration and evaluated through optical loss measurements, time-dependent loss (TiDL), temperature-dependent loss (TDL), and microstructural examination. The two chitosan types exhibited their lowest attenuation at a concentration of 0.04 g/mL, with AGC showing marginally lower optical loss, consistent with its higher purity and degree of deacetylation. AGC also demonstrated superior temporal and thermal stability, supported by SEM results indicating a smoother and more homogeneous core morphology. Nevertheless, SSC showed performance levels closely comparable to AGC, revealing that biowaste-derived chitosan can function effectively as a core material for large-core waveguides. This outcome underscores the potential of SSC as a sustainable, low-cost alternative, contributing to SDG 12 (Responsible Consumption and Production) through biowaste valorization, and SDG 9 (Industry, Innovation, and Infrastructure) by promoting eco-friendly materials for future optical sensor platforms. The results affirm that SSC-based waveguides hold promise for applications including humidity, pH, chemical, and biochemical sensing.

1. Introduction

Optical sensors have become one of the most rapidly developing technologies in modern measurement systems due to their high sensitivity, immunity to electromagnetic interference, and ability to perform remote and real-time monitoring. They operate based on changes in light properties when interacting with external stimuli, such as intensity, wavelength, or phase. This property makes them suitable for a wide range of applications such as in industries [1], biomedical diagnostics [2], and environmental monitoring [3].

Among various types of optical sensing devices, fiber-optic sensors are the most widely used because of their compact size, flexibility, and high signal-to-noise ratio [4]. Despite these advantages, fiber-optic sensors have inherent limitations, particularly bending losses, which occur when light escapes from the fiber core due to curvature [5], resulting in increased attenuation and reduced sensitivity. Additionally, the cylindrical geometry of optical fibers limits their integration into planar or chip-based systems [6], [7], while their fragile nature makes them less suitable for long-term use in harsh environments [8]. These challenges have motivated researchers to explore alternative light-guiding platforms that provide greater mechanical stability, lower optical loss, and better structural adaptability.

Optical waveguides have emerged as a promising alternative to overcome these limitations. In contrast to optical fibers, waveguides confine light within a thin core layer sandwiched between cladding materials, resulting in reduced bending losses and more controlled light propagation [9]. Their planar geometry allows easy integration with microfluidic and on-chip systems, making them highly compatible with modern photonic and sensing technologies. Furthermore, polymer optical waveguides offer key advantages including fast optical response, high sensitivity, mechanical flexibility, low cost, and ease of fabrication, making them well suited for a wide range of sensing and communication applications [10]. However, most reported optical waveguide sensors employ small core diameters [11, 12, 13] that demand precise alignment, making light coupling difficult and significantly limiting interaction with the

external environment. These constraints reduce their practicality for low-cost, disposable, or highly interactive sensing applications.

To address these limitations, polymer-based large-core optical waveguides (PLCOWs) have attracted increasing attention. Owing to their larger guiding dimensions, PLCOWs provide easier light coupling, higher tolerance to misalignment, and improved mechanical robustness. Their expanded guiding region enhances evanescent-field interaction, making them highly effective for chemical and environmental sensing applications. PLCOWs can be produced through a wide range of straightforward and cost-effective fabrication methods. These include molding injection [14], engraving [15] as well as emerging additive-manufacturing approaches such as 3D printing [16]. Beside their flexible fabrication routes, PLCOWs can also be formed from inexpensive polymers, such as NOA [17], elastomer [18], and UV resin [16]. This combination of versatile fabrication techniques and low-cost materials enables scalable and economically viable manufacturing of large-core polymer waveguides.

In addition to synthetic polymers, natural biopolymers have gained increasing attention due to their sustainability and attractive functional properties. Several biopolymers have been explored for optical and photonic applications, such as methylcellulose and methylcellulose–alginate composites, which have been implemented in optical humidity sensors [19]. Biopolymers have also found use in photomedicine, where Nizamoglu et al. [20] demonstrated their effectiveness for light delivery in deep tissues. Furthermore, cellulose-based materials have been successfully developed into biodegradable optical fibers, highlighting the expanding role of biopolymers in optical waveguiding technologies [21]. Among them, chitosan stands out as a biodegradable and biocompatible polymer capable of forming transparent thin films with tunable optical and chemical properties [22, 23]. Its intrinsic sensitivity to humidity [24], pH [25], and metal ions [26] provides strong potential for sensing applications. These attributes suggest that chitosan could serve not only as a functional sensing layer but also as a promising material for optical waveguide cores.

Despite these advantages, the use of chitosan as a guiding core material in large-core optical waveguides remains largely unexplored. Most existing studies have focused on employing chitosan as a functional cladding or coating layer rather than as the guiding core itself [23, 27, 28]. Therefore, the potential of chitosan to function directly as a waveguide core material particularly in large-core configurations has not been systematically investigated. Systematic comparisons between chitosan derived from industrial waste, such as shrimp shell waste, and high-purity analytical-grade chitosan are particularly limited. This comparison is important because waste-derived chitosan offers advantages in sustainability and cost efficiency, although its optical performance may be influenced by variations in material characteristics arising from raw material sources and processing routes.

Motivated by these considerations, this study investigates the feasibility of using chitosan as a core guiding material for large-core optical waveguides by evaluating the performances of waveguides fabricated using shrimp-shell-derived chitosan (SSC) and analytical-grade chitosan (AGC). The comparison includes optical loss, long-term temporal stability, temperature-dependent performance, and microstructural morphology. Through this approach, the study aims to evaluate the practicality of chitosan particularly waste-derived chitosan as a sustainable core material for future optical sensing applications, including humidity, pH, chemical, and biochemical detection.

2. Methods

2.1 Waveguide Fabrication

The optical waveguide was fabricated in a buried square core (BSC) structure using polymethyl methacrylate (PMMA) as the cladding material and chitosan as the optical guiding core. The fabrication process is illustrated schematically in Figure 1. The chitosan used in this study was obtained from shrimp shell waste (SSC) that had been processed into powder form. Two types of chitosan were investigated in this study: shrimp-shell-derived chitosan (SSC) and analytical-grade chitosan (AGC). The SSC was obtained from shrimp shell waste that had been processed into powder form, while the AGC used was medium molecular weight chitosan purchased from Sigma-Aldrich. No additional purification steps were applied to either material in order to preserve their original characteristics and enable a direct comparison. To prepare the core solution, 2.0–4.5 g of chitosan powder (in increments of 0.5 g) was dissolved in 50 mL of 10% acetic acid, as shown in Figure 1(a). The mixture was stirred at 400 rpm using a magnetic stirrer at room temperature for 1 hour until a homogeneous gel was formed. The solution was then subjected to ultrasonic filtering to remove air bubbles and ensure uniformity, as shown in Figure 1(c). The same procedure and composition variations were also AGC to enable direct comparison between both materials. The AGC used was Chitosan medium molecular weight from Sigma Aldrich.

As shown in Figure 1(d), PMMA sheet was cut into dimensions of 40 mm × 20 mm, and a straight channel was engraved at the center using a Computer Numerical Control (CNC) machine. The channel dimensions were designed to form a waveguide core path with a width of 1 mm, a depth of 1 mm, and a total length of 40 mm.

The prepared chitosan solution with the desired concentration was then poured into the groove, as shown in Figure 1(e). The solution was filled carefully using a micropipette to prevent air bubble formation and ensure a uniform surface. A polymer optical fiber (POF) was then aligned at both ends of the channel to facilitate optical coupling between the light source

and detector. The filled substrate was left to dry at room temperature for 24 hours, allowing solvent evaporation and solidification of the chitosan core.

Once the core layer was completely dried, an unengraved PMMA sheet of the same size was placed on top to serve as the upper cladding, as illustrated in Figure 1(f). The upper and lower PMMA layers were bonded using a thin layer of transparent optical adhesive to form a compact, enclosed planar waveguide. The final structure consisted of a 1 mm × 1 mm chitosan core embedded between two PMMA cladding layers, with the POFs connected at both ends for optical testing as shown in Figure 1(g). This configuration ensured efficient light confinement through total internal reflection and provided mechanical stability during subsequent optical characterization.

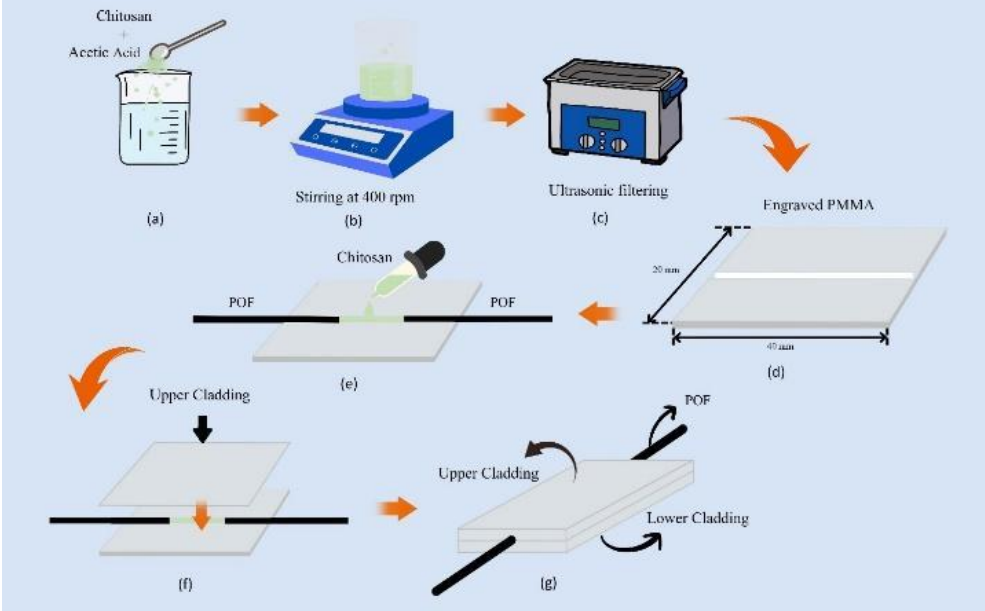

Fig. 1: Fabrication steps of the PMMA–chitosan optical waveguide: (a) Preparation of chitosan acetic acid mixture; (b) Stirring the chitosan solution at 400 rpm; (c) Ultrasonic filtering; (d) CNC-engraved PMMA substrate; (e) Filling the groove with chitosan gel and aligning POF; (f) Placement of upper cladding and (g) Final assembled waveguide structure.

2.2 Optical Characterization

The optical performance of the fabricated waveguides was evaluated by measuring optical power loss, time-dependent loss (TiDL), and temperature-dependent loss (TDL) using a 660 nm LED light source (IF-E97) and a photodiode detector (IF-D91B) connected to an Arduino-based optical power meter, as shown in Figure 2. The LED and photodiode were powered through the Arduino board, and the entire setup was aligned to ensure maximum coupling efficiency between the optical fiber and the waveguide.

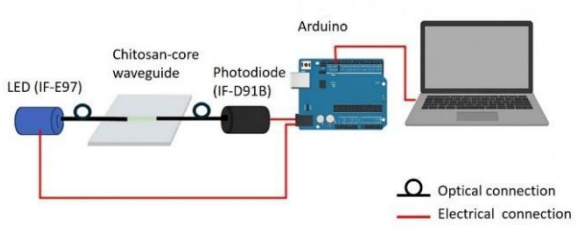

Fig. 2: Measurement set up for characterization of the waveguide

The measurement was repeated eight times for each concentration to ensure data consistency, and the mean value was used for analysis. The resulting data were plotted as average optical loss versus chitosan concentration to determine the optimum composition providing minimum attenuation.

2.2.1 Optical Loss Measurement

To study the effect of chitosan concentration on optical loss, waveguides were fabricated using both analytical-grade and waste-derived chitosan with varying concentrations (2.0–4.5 g per 50 mL). For each sample, the input optical power (P_{in}) and output optical power (P_{out}) were recorded using the optical power meter. The optical loss (L)was calculated using the logarithmic power ratio between the input and output signals, expressed as:

$$L(dB) = \left|10log_{10}(\frac{P_{out}}{P_{in}})\right| \quad (1)$$

2.2.2 Time-Dependent and Temperature-Dependent Characterization

The stability of light propagation through the fabricated waveguide was evaluated using Time-Dependent Loss (TiDL) measurements. This characterization aimed to observe variations in optical power loss over time and to assess the structural and environmental stability of the chitosan core material. Optical transmission was monitored for 168 hours under two different environmental conditions: air and water. For TiDL measurements in

aqueous conditions, distilled water (aquades) was used as the immersion medium. The use of aquades was intended to reduce the influence of dissolved impurities compared to tap water, while maintaining experimental simplicity and reproducibility. Linear regression was applied to determine the rate of change of optical loss with respect to time (dB/hour).

The TiDL measurements were conducted as a continuous single-run experiment for each waveguide configuration. Optical transmission was monitored continuously over a 168-hour period without resetting or repeating the experiment. The reported TiDL values were obtained from linear regression of the time-series optical loss data.

To evaluate the thermal stability of the waveguide, Temperature-Dependent Loss (TDL) measurements were performed. The optical power loss was recorded while the ambient temperature varied from 30°C to 60°C in increments of 5°C using a digitally controlled hot plate. The The TDL value was determined from the slope of the linear regression between optical power loss and temperature.

3. Results and Discussion

3.1. Effect of Chitosan Concentration on Optical Loss

Optical power loss measurements for both waste-derived and analytical-grade chitosan cores were performed using uncladded waveguides. This characterization was intended to assess the intrinsic optical loss behavior when the core is directly exposed to the environment, mimicking conditions in sensing applications. For each concentration, the average optical loss obtained from eight repeated measurements was plotted in Figure 3, with a maximum relative standard deviation (RSD) below 0.2%, indicating high precision measurement. The results demonstrate that optical loss increases with increasing chitosan concentration, suggesting that higher concentrations lead to less uniform and optically favorable core structures, thereby enhancing scattering and absorption losses.

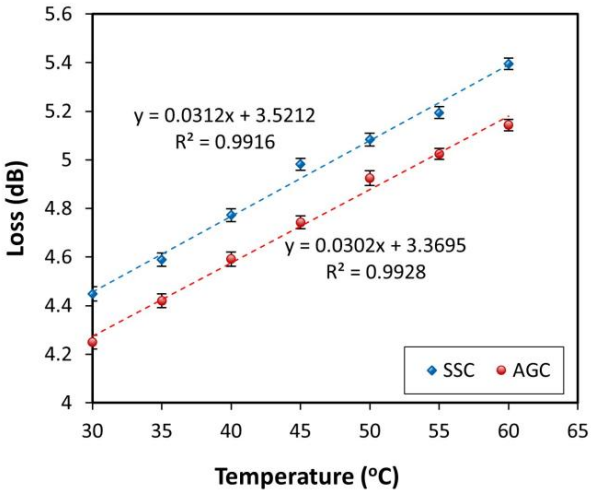

Fig. 3: Optical loss of uncladded waveguides fabricated using shrimp-shell-derived chitosan (SSC) and analytical-grade chitosan (AGC) at different chitosan concentrations.

At low concentration (0.04 g/mL), both materials achieve the lowest loss values, with analytical-grade chitosan performing slightly better. Conversely, the highest losses are observed at the maximum concentration (0.09 g/mL), again for both materials. While the optical loss values of waste-derived chitosan are consistently higher, the difference between the two materials remains relatively small across the concentration range, demonstrating that waste-derived chitosan can provide an optical performance comparable to that of analytical-grade material.

The power loss of the chitosan-core waveguide is comparable to that of other large-core optical waveguides reported in the literature. When compared with an unsaturated polyester resin (UPR)–based waveguide [29], the chitosan waveguide exhibits approximately 84% lower optical loss. In addition, relative to waveguides employing Norland Optical Adhesive (NOA) photopolymer as the core material [30], the chitosan waveguide achieves more than 37% lower loss, demonstrating its strong potential as a low-loss, biopolymer-based alternative for optical guiding applications.

The observed optical loss behavior can be attributed to a combination of refractive-index inhomogeneity, scattering mechanisms (Rayleigh/Mie regimes) associated with microvoids and porosity, and absorption related to hydroxyl (–OH) functional groups inherent to chitosan, particularly under humid or elevated temperature conditions.

For subsequent TiDL and TDL characterizations, a chitosan concentration of 0.04 g/mL was selected as the optimal composition for both SSC and AGC waveguides. This concentration exhibited the lowest optical loss among all tested variations, with the waste-derived chitosan waveguide achieving a minimum loss of 4.284 dB. The superior performance at this concentration indicates that lower chitosan loading promotes better optical uniformity and reduces scattering sites within the core, making it the most suitable formulation for evaluating the waveguide's temporal and thermal stability.

The waveguide structure relies on the refractive-index contrast between the chitosan core and the PMMA cladding to achieve total internal reflection. PMMA, with its well-established refractive index in the visible range, serves as an effective cladding material to confine light within the chitosan core. Although direct refractive-index measurements of SSC and AGC were not conducted, stable optical guiding observed experimentally confirms sufficient index contrast for waveguiding. The discussion of optical loss in relation to material uniformity and purity is based on a comparative assessment of material grade and standardized specifications rather than absolute chemical purity values. In this study, the AGC was a commercially available chitosan (medium molecular weight) supplied by Sigma-Aldrich, characterized by a specified degree of deacetylation of ≥ 75% and a controlled viscosity

range of 200–800 cps (1% in acetic acid), as provided in the manufacturer's specification sheet.

These standardized parameters indicate a relatively consistent chemical composition and processing quality, which are known to promote more homogeneous film formation and stable optical behavior. In contrast, SSC, obtained through a laboratory-scale extraction process, is more susceptible to variations in processing conditions and residual constituents. Consequently, the observed differences in optical performance and microstructural morphology are interpreted in the context of differences in material grade, processing route, and structural uniformity, rather than direct chemical purity measurements.

3.2. Time Dependent Loss (TiDL)

The TiDL characterization was performed over 168 hours in both air and water environments to assess the long-term stability of the chitosan-core waveguides.As shown in Figures 4, the optical power loss increased linearly with time for all samples. In air, the TiDL rates were for AGC, 6.3×10^{-3} dB/h for SSC and 5.3×10^{-3} dB/h for AGC indicating that both materials exhibit comparable stability under ambient conditions. The relative standard deviation (RSD) of the data is shown as error bars in the graph. The maximum RSD for both SSC and AGC is 0.03%.

In contrast, immersion in water resulted in a substantial increase in TiDL, reaching 8.5×10^{-3} dB/h for SSC and 7.9×10^{-3} dB/h for AGC, as shown in Figure 4(b). This increase is attributed to the hygroscopic nature of chitosan, which readily absorbs water molecules, causing refractive-index changes and structural swelling [31]. Such changes weaken total internal reflection (TIR) and increase propagation loss. Notably, this inherent sensitivity of chitosan to humidity and fluid uptake, though unfavorable for stability, provides a valuable mechanism for optical sensing. Variations in absorbed water or liquid analytes modulate the effective refractive index and geometry of the core, creating measurable changes in guided light intensity. This principle enables applications such as humidity sensing, liquid detection, biosensing, and chemical sensing, particularly for analytes that interact with chitosan through hydrogen bonding, ionic binding, or swelling responses.

These findings clearly demonstrate that humidity and moisture absorption strongly affect the optical performance of chitosan-based waveguides. Consequently, incorporating a protective PMMA cladding layer is essential to enhance stability for conventional waveguiding applications, whereas keeping the waveguide partially or fully uncladded is advantageous for sensing platforms.

The characterization was further extended by evaluating the TiDL of the cladded chitosan-core waveguide over a 168-hour observation period in an air environment. This measurement aimed to assess the temporal stability of the encapsulated structure under ambient conditions. The resulting TiDL trend for the cladded waveguide is shown in Figure 5. The RSD for the cladded waveguide is 0.06% which is within acceptable range.

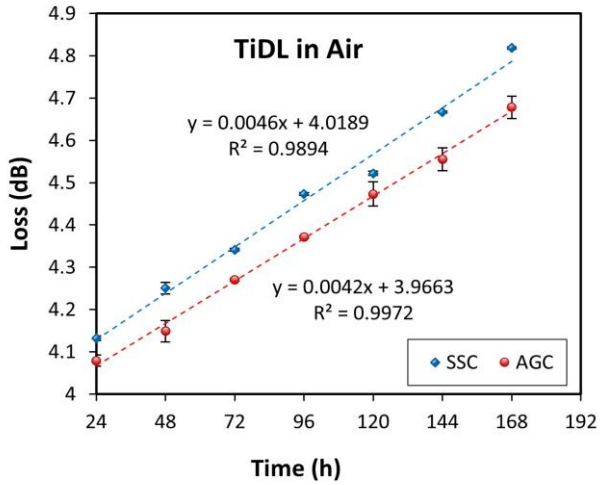

(a)

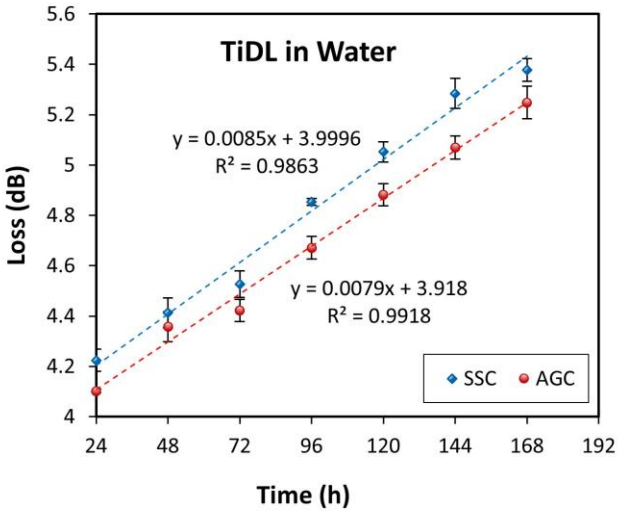

(b)

Fig. 4: Time-dependent loss (TiDL) of uncladded chitosan-core waveguides measured in air over seven days for shrimp-shell-derived chitosan (SSC) and analytical-grade chitosan (AGC) in (a) air and (b) water.

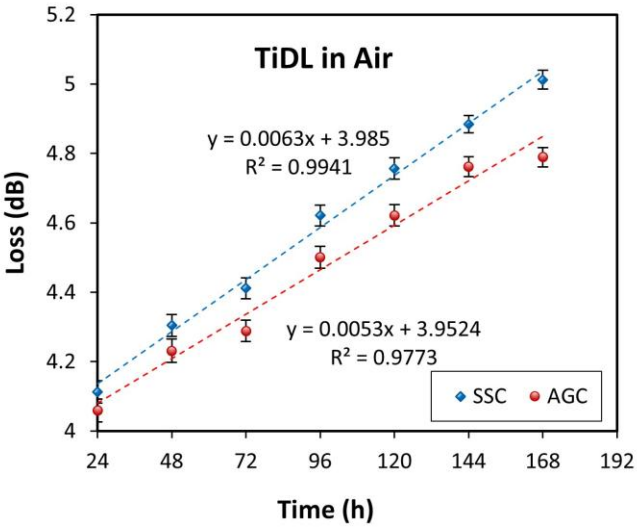

(a)

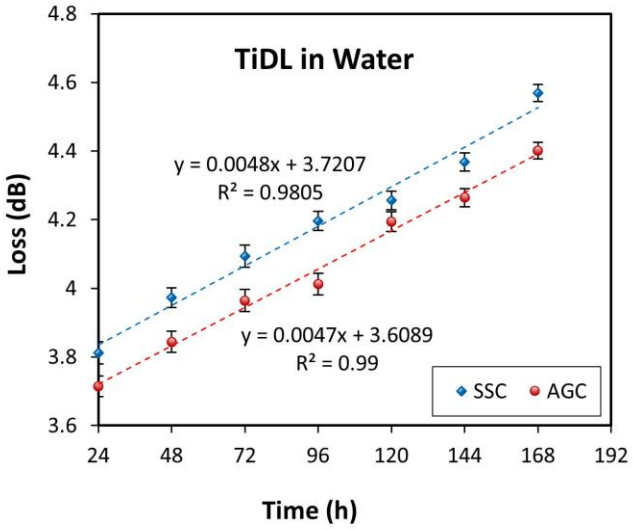

(b)

Fig. 5: Time-dependent loss (TiDL) of cladded chitosan-core waveguides measured in air over seven days for SSC and AGC in (a) air and (b) water

The optical loss measurements of the chitosan-core waveguides with PMMA cladding demonstrated a significant reduction in the TiDL compared to the uncladded configuration. As shown in Figure 5(a), the cladded waveguide exhibited TiDL values of 4.6 × 10^{-3} dB/h for SSC and 4.2 × 10^{-3} dB/h for AGC in air. When immersed in water, the loss rates increased slightly due to moisture interaction, with SSC showing 4.8 × 10^{-3} dB/h and AGC 4.7 × 10^{-3} dB/h, as presented in Figure 5(b). The application of the cladding layer substantially enhanced waveguide stability in both environments by suppressing direct environmental interaction and minimizing scattering losses. Relative to the uncladded waveguides, the TiDL values in air decreased by 26.9% for SSC and 20.8% for AGC, while in water the reductions reached 43.5% and 40.5%, respectively, confirming the effectiveness of PMMA encapsulation in improving long-term optical performance.

These results indicate that one of the most effective strategies for reducing optical loss in chitosan-based waveguides is to prevent direct contact between the chitosan core and water. This is consistent with the notable decrease in optical loss observed after applying the cladding layer. Another potential approach to improve waveguide stability is to increase the degree of deacetylation (DD) of the chitosan material. As reported by Mathaba & Daramola (2020), chitosan with a higher DD exhibits greater water resistance and is less prone to dissolution. This trend aligns with the findings of the present study, in which analytical-grade chitosan, typically characterized by a higher DD, showed lower optical loss compared to waste-derived chitosan, which generally possesses a lower DD value. In addition, material reinforcement through doping has also been reported as an effective method to enhance chitosan durability. For example, cobalt and nitrogen co-doped (CoNC) materials have been shown to suppress oxidation reactions in chitosan, thereby improving its chemical stability [33], [34].

3.3. Temperature Dependent Loss (TDL)

The TDL measurements were conducted during a monotonic temperature increase. Cooling cycles were not performed; therefore, the reversibility of temperature-induced optical loss was not evaluated in this study. As shown in Figure 6, the TDL data show that the uncladded waveguides have higher temperature sensitivity than the cladded devices. The measured TDL were 0.0392 dB/°C (SSC) and 0.0375 dB/°C (AGC) for the uncladded cores, decreasing to 0.0312 dB/°C (SSC) and 0.0302 dB/°C (AGC) after PMMA encapsulation. The increase of optical loss with temperature is primarily caused by the thermo-optic effect (temperature dependence of refractive index) [35] and by thermomechanical expansion of the polymer matrix, both of which alter mode confinement and increase scattering/attenuation in polymer waveguides.

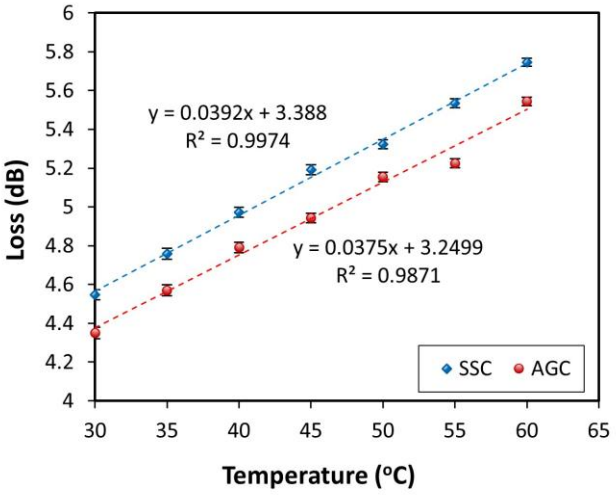

(a)

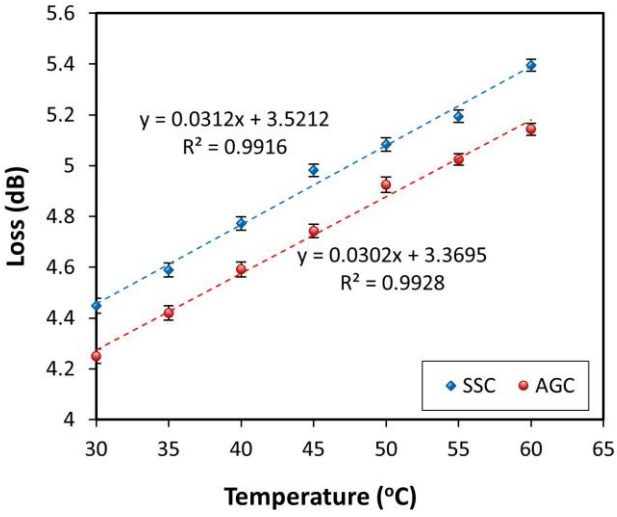

(b)

Fig. 6 : Temperature-dependent loss (TDL) of SSC and AGC chitosan-core of (a) uncladded waveguide and (b) cladded waveguide.

Comparing SSC and AGC, SSC consistently exhibits slightly higher TDL than AGC. This difference is consistent with material quality and hygroscopic behavior. Waste-derived chitosan typically contains more residual impurities and a lower DD, which increase water uptake and microstructural heterogeneity [36], [37]; thermally driven redistribution of absorbed moisture and relaxation of microvoids therefore produces larger refractive-index perturbations in SSC than in AGC.

Encapsulation with PMMA reduces the TDL for both materials because the cladding provides several stabilizing effects on the waveguide structure. It mechanically constrains the thermal expansion of the chitosan core, which helps maintain the geometrical and optical integrity of the guiding region as temperature increases. The cladding also minimizes direct exposure of the hygroscopic chitosan to ambient humidity and temperature fluctuations, thereby reducing moisture-induced refractive-index variations that typically worsen at elevated temperatures. In addition, the presence of the PMMA layer alters the effective thermo-optic response of the waveguide by blending the thermo-optic coefficients of the core and cladding materials, resulting in a more stable and less temperature-sensitive guided mode.

SEM images were acquired from multiple regions of each waveguide core to ensure representative observation of surface morphology. The SEM analysis was qualitative in nature and focused on comparative morphological features rather than quantitative roughness or porosity measurements. The SEM images support these findings by revealing substantial microstructural differences between SSC and AGC both before and after TDL characterization, as shown in Figure 7. Figures 7(a) and 7(b) show the morphology of SSC before and after TDL characterization. Before testing, SSC displays a more irregular, fragmented, and heterogeneous structure with noticeable debris and flake-like formations. This morphology reflects the lower purity and lower DD of waste-derived chitosan, which commonly contains residual minerals and proteins that hinder uniform film formation. After TDL characterization (Figure 7(b)), the SSC surface appears further degraded, with more pronounced cracking, particle agglomeration, and increased porosity.

Figures 8 illustrate the surface morphology of AGC. Prior to TDL characterization (Figure 8(a)), AGC exhibits a relatively smooth and compact structure with fewer voids and cracks, indicating a more homogeneous film formation. This morphology is consistent with the higher purity and DD typically associated with analytical-grade chitosan, which promotes improved intermolecular interaction and film uniformity. After TDL characterization (Figure 8(b)), minor surface roughening is observed, along with the appearance of small pores and microcracks. These changes suggest slight moisture absorption and structural relaxation during prolonged exposure, which may contribute to the gradual increase in optical loss observed during TiDL measurements. Therefore, the SEM results confirm that material purity and structural integrity strongly influence optical performance. AGC demonstrates better stability and smoother microstructure, which correlate with lower optical loss and slower degradation over time. In contrast, SSC undergoes greater morphological deterioration during TDL exposure, consistent with its higher optical losses and stronger sensitivity to environmental humidity.

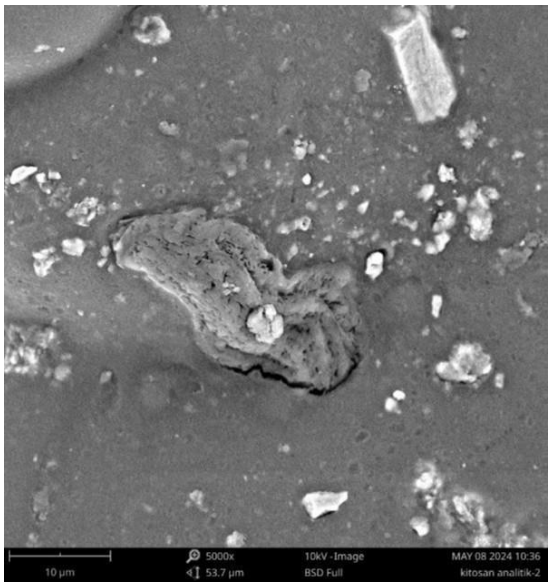

(a)

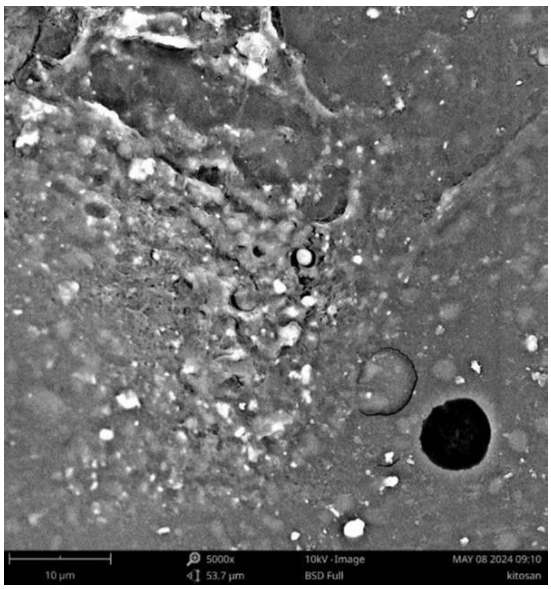

(b)

Fig. 7: SEM images of SSC (a) before and (b) after TDL characterization.

The TDL behavior of the chitosan-based waveguides can be directly linked to the thermal degradation mechanisms of chitosan. As reported by [38], chitosan undergoes a two-stage degradation process, in which the secondary degradation of acetylated units becomes more significant at lower DD. This mechanism explains the microstructural irregularities observed in the SEM images of samples

with higher TDL values, where localized degradation may lead to microvoid formation and surface roughening. Conversely, samples with smoother SEM morphology exhibit lower TDL, indicating greater thermal stability and reduced scattering. These observations highlight the strong interplay between thermal degradation kinetics, microstructural integrity, and temperature-dependent optical performance of chitosan-based waveguides.

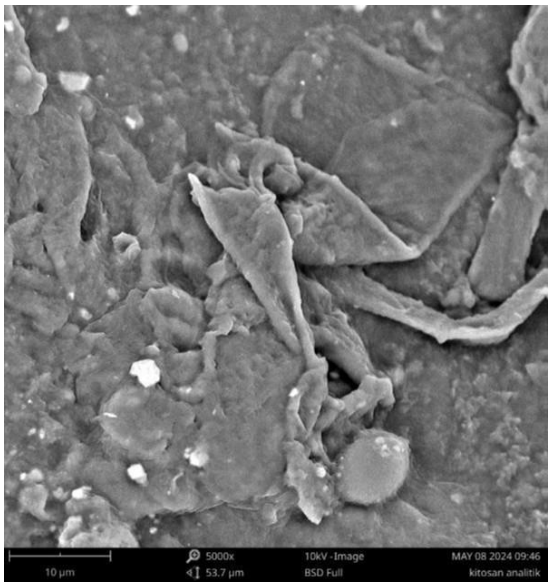

(a)

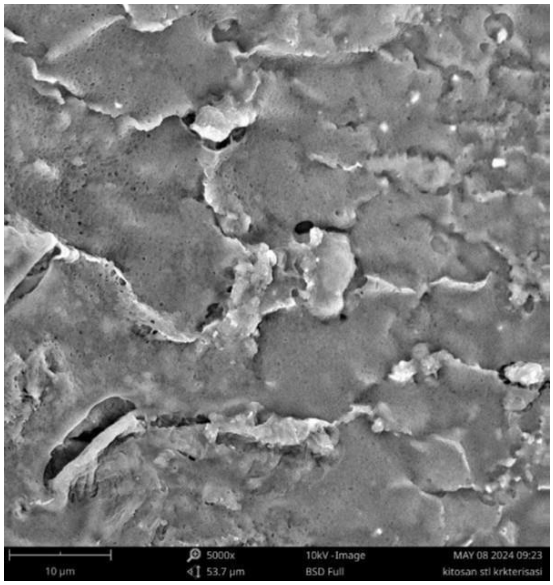

(b)

Fig. 8: SEM images of AGC (a) before and (b) after TDL characterization.

In addition to the qualitative morphological differences observed in the SEM images, a rough quantitative porosity analysis was performed to further correlate microstructure with optical performance. The porosity values were estimated from SEM micrographs using ImageJ software through grayscale thresholding and area fraction analysis. The AGC waveguide exhibited an initial porosity of 8.319%, which increased to 14.686% after TDL characterization. In contrast, the SSC waveguide showed a higher initial porosity of 12.613%, which further increased to 21.624% after thermal exposure.

The consistently higher porosity of SSC indicates a less compact microstructure and a higher density of scattering sites, which explains the higher optical loss and stronger temperature-dependent loss observed in SSC-based waveguides. The increase in porosity after TDL characterization suggests thermally induced microvoid formation and structural relaxation, which further degrade light confinement through increased scattering and refractive-index inhomogeneity.

Overall, the results indicate that the SSC-based waveguide shows performance comparable to the AGC-based device, despite the lower material purity typically associated with waste-derived chitosan. The relatively small difference in TDL and optical loss demonstrates that SSC remains a promising and cost-effective alternative for optical sensing platforms. Given its intrinsic hygroscopicity, pH-responsiveness, and ability to undergo reversible refractive-index changes, a chitosan-core waveguide, whether derived from analytical-grade or waste sources, has strong potential for further development into various sensing applications, including humidity sensing, pH detection, biochemical sensing, metal-ion detection, and volatile organic compound (VOC) monitoring. These findings highlight the feasibility of advancing SSC-based waveguides as sustainable, low-cost, and environmentally friendly optical sensors.

4. Conclusions

This work presents a comparative evaluation of shrimp-shell-derived chitosan (SSC) and analytical-grade chitosan (AGC) as core materials for large-core optical waveguides. Although AGC demonstrates slightly better performance, reflected in lower optical loss, improved TiDL and TDL stability, and a more uniform microstructure, its advantages primarily stem from its higher purity and degree of deacetylation. SEM observations confirm that SSC possesses a marginally rougher morphology, which contributes to increased scattering and explains its slightly higher attenuation. Despite these differences, the overall performance gap between SSC and AGC is small, indicating that SSC remains capable of supporting stable light propagation suitable for optical sensing applications.

Importantly, the successful implementation of SSC underscores its value as a sustainable low-cost material. Its use contributes to SDG 12 (Responsible Consumption and Production) by converting shrimp-shell waste into functional photonic components, and advances SDG 9 (Industry, Innovation, and Infrastructure) by promoting eco-friendly materials for optical sensor development. Given its biodegradability, accessibility, and competitive optical performance, SSC shows strong potential for future waveguide-based sensors, including humidity, pH, chemical, biochemical, and heavy-metal detection. Overall, the findings affirm that waste-

derived chitosan is a viable and sustainable alternative to analytical-grade chitosan for large-core optical waveguide applications.

Acknowledgement

We would like to thank the Faculty of Mathematics and Natural Sciences, Universitas Negeri Semarang, for funding the research through grant number 50.21.4/UN37/PPK.04/2025. Our gratitude also goes to the members of the Physics Department, Universitas Negeri Semarang for their helpful discussion throughout the completion of this work.

References

[1] Y. H. Kadhum, A. M. Salman, and A. Al-Janabi, "Compact High-Sensitive Mach–Zehnder-Based Optical Fiber Sensor for Monitoring Gaseous Acetone Concentrations" Opt. Fiber Technol., 95, 104422, (2025).

[2] M. Ashraf and K. K. Qureshi, "Optical Fiber Sensors in Biomedical: Trends and Emerging Research—A Review" Opt. Fiber Technol., 95, 104404, (2025).

[3] N. N. Zulkeflee, S. H. M. Saing, Y. M. Kamil, M. Mansor, N. A. Halim, N. H. Z. Abidin, and M. A. Mahdi, "Multimode Tapered Fiber Sensor-Based Optical Response for the Detection of Nile Red-Stained Microplastics" Opt. Fiber Technol., 95, 104441, (2025).

[4] R. K. Gangwar, A. K. Pathak, F. Chiavaioli, M. A. Bakar, Y. M. Kamil, M. A. Mahdi, and V. K. Singh, "Optical Fiber SERS Sensors: Unveiling Advances, Challenges, and Applications in a Miniaturized Technology" Coord. Chem. Rev., 510, 215861, (2024).

[5] S. Hussain, L. Liu, M. Rui, Z. Yuanxiang, A. Ghaffar, G. Y. Chen, H. M. Alshehri, K. K. Qureshi, K. Ali, B. Das, and M. Mehdi, "POF Helical Sensor: A Simple Design Approach for Vibration Measuring Based on Bend Loss Coupling" Opt. Express., 32(26), 46763–46775, (2024).

[6] X. Mu, S. Wu, L. Cheng, and H. Y. Fu, "Edge Couplers in Silicon Photonic Integrated Circuits: A Review" Appl. Sci., 10(4), 1538, (2020).

[7] S. Khan, S. M. Buckley, J. Chiles, R. P. Mirin, S. W. Nam, and J. M. Shainline, "Low-Loss, High-Bandwidth Fiber-to-Chip Coupling Using Capped Adiabatic Tapered Fibers" APL Photon., 5(5), 056101, (2020).

[8] S. N. Khonina, N. L. Kazanskiy, and M. A. Butt, "Optical Fibre-Based Sensors—An Assessment of Current Innovations" Biosensors., 13(9), 835, (2023).

[9] S. K. Selvaraja and P. Sethi, "Review on optical waveguides" Emerging Waveguide Technology, 95, 458, (2018).

[10] C. A. Zimmermann, K. N. Amouzou, and B. Ung, "Recent Advances in PDMS Optical Waveguides: Properties, Fabrication, and Applications" Adv. Opt. Mater., 13(1), 2401975, (2025).

[11] C. Peng, C. Yang, H. Zhao, L. Liang, C. Zheng, C. Chen, L. Qin, and H. Tang, "Optical Waveguide Refractive Index Sensor for Biochemical Sensing" Appl. Sci., 13(6), 3829, (2023).

[12] R. Kinoshita and T. Ishigure, "Optimum Core Structural Design of Polymer Optical Waveguides as Edge Couplers for Co-Packaging" Opt. Express., 32(14), 24415–24431, (2024).

[13] S. Suda, A. Noriki, H. Kuwatsuka, F. Nakamura, Y. Atsumi, T. Kurosu, T. Murao, and T. Amano, "High-Power Stability and Reliability of Polymer Optical Waveguide for Co-Packaged Optics" J. Lightwave Technol., 43(10), 4903–4912, (2025).

[14] H. J. Park, K. S. Lim, and H. S. Kang, "Low-Cost 1×2 Plastic Optical Beam Splitter Using a V-Type Angle Polymer Waveguide for Automotive Networks" Opt. Eng., 50(7), 075002, (2011).

[15] V. Prajzler, M. Neruda, and J. Špirková, "Planar Large-Core Polymer Optical 1×2 and 1×4 Splitters Connectable to Plastic Optical Fiber" Radioengineering., 22(3), 751–757, (2013).

[16] R. Oliveira, R. Nogueira, and L. Bilro, "Do-It-Yourself Three-Dimensional Large-Core Multimode Fiber Splitters Through a Consumer-Grade 3D Printer" Opt. Mater. Express., 12(2), 593–605, (2022).

[17] V. Prajzler, M. Knietel, and R. Maštera, "Large-Core Optical Planar Splitter for Visible and Infrared Region" Opt. Quantum Electron., 48(2), 155, (2016).

[18] V. Prajzler and J. Zavřel, "Large-Core Optical Elastomer Splitter Fabricated Using 3D Printing Pattern" Opt. Quantum Electron., 53(6), 337, (2021).

[19] J. Patrakka, V. Hynninen, P. Huttunen, and Nonappa, "Biopolymer Optical Fibers for High-Sensitivity Quantitative Humidity Monitoring" ACS Appl. Mater. Interfaces., 17(35), 49816–49828, (2025).

[20] S. Nizamoglu, M. C. Gather, M. Humar, M. Choi, S. Kim, K. S. Kim, S. K. Hahn, G. Scarcelli, M. Randolph, R. W. Redmond, and S. H. Yun, "Bioabsorbable Polymer Optical Waveguides for Deep-Tissue Photomedicine" Nat. Commun., 7(1), 10374, (2016).

[21] M. Reimer, D. Van Opdenbosch, and C. Zollfrank, "Fabrication of Cellulose-Based Biopolymer Optical Fibers and Their Theoretical Attenuation Limit" Biomacromolecules., 22(8), 3297–3312, (2021).

[22] A. Y. Mironenko, A. A. Sergeev, A. E. Nazirov, E. B. Modin, S. S. Voznesenskiy, and S. Y. Bratskaya, "H_2S Optical Waveguide Gas Sensors Based on Chitosan/Au And Chitosan/Ag Nanocomposites" Sens. Actuators B Chem., 225, 348–353, (2016).

[23] E. H. Ahmed, A. I. Hashem, M. Adlung, C. Wickleder, M. M. H. Ayoub, I. K. Battisha, and A. Amin, "Tailoring Chitosan Nanocomposites for Planar Optical Waveguide Applications" Polym. Sci. Ser. A., 64(4), 342–353, (2022).

[24] P. Kumari, A. Kumar, A. Yadav, G. Gupta, G. Gupta, D. D. Shivagan, and K. Bapna, "Chitosan-Based Highly Sensitive Viable Humidity Sensor for Human Health Monitoring" ACS Omega., 8(42), 39511–39522, (2023).

[25] R. Hosseinlou, M. Dargahi, and A. Keshtkar Vanashi, "Alkaline-Range pH Sensor Based on Chitosan Hydrogel: A Novel Approach to pH Sensing" Int. J. Biol. Macromol., 279, 135199, (2024).

[26] R. Borgohain, P. K. Boruah, and S. Baruah, "Heavy-Metal Ion Sensor Using Chitosan-Capped ZnS Quantum Dots" Sens. Actuators B Chem., 226, 534–539, (2016).

[27] X. Xue, Y. Guo, F. Yan, N. Alisher, and J. Li, "Compact Fabry–Perot Microcavity-Based Fiber-Optic Humidity Sensor Constructed by Hollow-Core Fiber and Chitosan Film" Chem. Phys. Lett., 883, 142537, (2026).

[28] C. Teng, R. Yang, S. Ying, H. Xia, Y. Zhang, L. Shi, S. Deng, Z. Chen, H. Qiao, and L. Yuan, "Chitosan/Polyacrylic Acid Functionalized Side-Polish Polymer Optical Fiber-Based SPR Sensor for Cu^{2+} Ion Detection" Photonics., 12(5), 461, (2025).

[29] I. Yulianti, N. M. Dharma Putra, B. Astuti, K. E. Kurniansyah, and Z. A. F. Latif, "Fabrication and Characterization of Polyester/Polymethylmethacrylate Buried Waveguide for Operation in Visible Light Range," in AIP Conf. Proc., 2169(1), 060006, (2019).

[30] V. Prajzler, P. Kulha, M. Knietel, and H. Enser, "Large-Core Plastic Planar Optical Splitter Fabricated by 3D Printing Technology" Opt. Commun., 400, 38–42, (2017).

[31] Y. Chen, Q. Duan, L. Yu, and F. Xie, "Thermomechanically Processed Chitosan: Gelatin Films with Improved Transparency and Mechanical Robustness" Carbohydr. Polym., 272, 118522, (2021).

[32] M. Mathaba and M. O. Daramola, "Effect of Chitosan Degree of Deacetylation on the Performance of PES Membranes during AMD Treatment" Membranes., 10, 52, (2020).

[33] S. Xie, S. Huang, W. Wei, X. Yang, Y. Liu, X. Lu, and Y. Tong, "Chitosan Waste-Derived Co and N Co-Doped Carbon Electrocatalyst for Efficient Oxygen Reduction Reaction" ChemElectroChem., 2(11), 1806–1812, (2015).

[34] A. Khan, M. Goepel, J. C. Colmenares, and R. Gläser, "Chitosan-Based N-Doped Carbon Materials for Electrocatalytic and Photocatalytic Applications" ACS Sustain. Chem. Eng., 8(12), 4708–4727, (2020).

[35] Z. Zhang, P. Zhao, P. Lin, and F. Sun, "Thermo-Optic Coefficients of Polymers for Optical Waveguide Applications" Polymer., 47(14), 4893–4896, (2006).

[36] T. S. Trung, W. W. Thein-Han, N. T. Qui, C.-H. Ng, and W. F. Stevens, "Functional Characteristics of Shrimp Chitosan and its Membranes as Affected by Degree of Deacetylation" Bioresour. Technol., 97(4), 659–663, (2006).

[37] I. Thamer, M. Mazurek-Budzyńska, and V. Kumaravel, "Sustainable Biopolymer Design: Extraction of Chitin and Chitosan Using Natural Deep Eutectic Solvents" Mater. Des., 259, 114775, (2025).

[38] M. A. Gámiz-González, D. M. Correia, S. Lanceros-Mendez, V. Sencadas, J. G. Ribelles, and A. Vidaurre, "Kinetic Study of Thermal Degradation of Chitosan as a Function of Deacetylation Degree" Carbohydr. Polym., 167, 52–58, (2017).